ELSEVIER

Microporous and Mesoporous Materials 37 (2000) 209–222

MICROPOROUS AND MESOPOROUS MATERIALS

www.elsevier.nl/locate/micromeso

Study of the coordination of Cu^{2+} in zeolite Y: Interaction with water and ammonia

Annelies Delabie [a], Kristine Pierloot [a,*], Marijke H. Groothaert [b], Bert M. Weckhuysen [b], Robert A. Schoonheydt [b]

[a] *Department of Chemistry, K.U. Leuven, Celestijnenlaan 200F, 3001 Heverlee-Leuven, Belgium*
[b] *Centre for Surface Chemistry and Catalysis, K. U. Leuven, K. Mercierlaan 92, 3001 Heverlee-Leuven, Belgium*

Received 21 June 1999; received in revised form 11 October 1999; accepted for publication 11 October 1999

Abstract

The ligand field spectrum of Cu(II) exchanged zeolite Y, obtained after saturation with H_2O and NH_3 and during the gradual desorption of these ligands, was measured by diffuse reflectance spectroscopy (DRS). DFT and ab-initio calculations on several model clusters were performed to interpret the spectra. The structure of the model clusters was optimized by means of density functional theory (DFT), using the B3LYP functional. The electronic spectra of the models were calculated using multiconfigurational perturbation theory based on a CASSCF wavefunction (CASPT2) and compared with the DRS spectra. Firstly, several $[Cu(NH_3)_y(H_2O)_x]^{2+}$ complexes were studied. It was shown that in fully hydrated Cu(II)Y, a $[Cu(H_2O)_6]^{2+}$ complex can be present in the cages of the zeolite. In Cu(II)Y, saturated with NH_3, the $[Cu(NH_3)_4]^{2+}$ complex is present, but the Cu^{2+} center in this complex must still be coordinated to one or two lattice oxygens in the zeolite. Secondly, calculations were performed on large cluster models, representing the adsorption complexes of one H_2O or one NH_3 ligand on Cu^{2+} in the six-ring sites in zeolite Y. The ligand field spectrum of partially dehydrated and deammoniated Cu(II)Y shows d–d transitions at a lower energy than the spectrum of fully dehydrated Cu(II)Y, which is confirmed by the CASPT2 results of the six-ring clusters.

Keywords: Ab-initio methods; Adsorption of H_2O and NH_3; Cu(II) ions in zeolites; Diffuse reflectance spectroscopy

1. Introduction

Zeolites containing transition metal ions are widely studied, because of their interesting adsorptive and catalytic properties [1]. These ions, introduced into the zeolite by ion exchange, can occupy specific coordination sites after dehydration. The resulting coordination to the lattice oxygens is often unsaturated, leaving the possibility for adsorption of small molecules to the metal site. The knowledge of the coordination and electronic structure of the transition metal centers is important for the investigation of the catalytic potential of these materials.

X-ray diffraction (XRD) gives information about the location of the transition metal ions in the zeolite unit cell [2,3]. However, detailed information about the coordination of the metal cannot be obtained, since no distinction between silicon and aluminum atoms can be made, and the site

* Corresponding author. Fax: +32-16-327-992.
E-mail address: kristine.pierloot@chem.kuleuven.ac.be (K. Pierloot)

1387-1811/00/$ - see front matter
PII: S1387-1811(99)00267-X

structure is an average over occupied and non-occupied sites. Electronic spectroscopy provides an alternative way to study the coordination environment of transition metal ions in zeolites. The energy of the d–d transitions depends on the number and position of the ligands surrounding the transition metal ion (lattice oxygens in the case of zeolites). As such, these spectra provide a 'fingerprint' of the specific metal environment in the zeolite. The ligand field spectra can be measured experimentally by diffuse reflectance spectroscopy (DRS).

Recently, a combined DFT/ab-initio approach was applied to study the coordination of Co^{2+} and Cu^{2+} to six-ring sites in zeolites, as present in zeolite A and faujasite-type zeolites [4–6]. The structure of the local coordination environment of these metals and the corresponding ligand field spectrum were studied using large cluster models, including all six surrounding Si or Al tetrahedra, terminated by H or OH groups. Partial geometry optimizations using DFT (with the BP86 or B3LYP functional), provide an accurate coordination geometry. It was shown that, due to the strong tendency of the transition metal ion to maximize its coordination number, the six-rings are strongly distorted. In the case of Cu^{2+}, a fourfold coordination in the six-ring site was obtained. For Co^{2+}, a coordination to three, four or five oxygens, depending on the distribution of aluminums in the six-ring, may be reached. The electronic spectra of these structures were calculated using multiconfigurational perturbation theory, based on a complete active space SCF (CASSCF) wave function: the CASPT2 method. The calculated excitation energies of the optimized structures were in excellent agreement with the experimental band positions, confirming the quality of the optimized structures.

The next step is to study the adsorption of small probe molecules on these transition metal centers. In the present work, the interaction of H_2O and NH_3 with Cu^{2+} in the six-ring sites of zeolite Y is studied. The six rings are the preferred coordination sites for Cu^{2+} at small Cu^{2+} loadings [38,39]. In fully hydrated or ammoniated zeolites, it is generally accepted that the transition metal ions do not coordinate to lattice oxygens, and indeed their d–d and EPR (electron paramagnetic resonance) spectra closely resemble those obtained in solution [7]. Infra-red (IR) and EPR studies revealed a $[Cu(NH_3)_4]^{2+}$ complex in Cu(II)Y saturated with NH_3, and this complex is proposed to be the active catalyst for reduction of NO with NH_3 [8–10]. The influence of the zeolite environment on the $[Cu(NH_3)_4]^{2+}$ complex has been studied by Raman spectroscopy [11]. In completely hydrated Cu(II)Y, the $[Cu(H_2O)_6]^{2+}$ complex in the supercage is identified [7,12–14]. This complex has been observed not only in zeolite Y, but also in other hydrated Cu^{2+} zeolites, for example in Cu—ZSM-5 and in Cu—mordenite [12,15–18]. Upon controlled dehydration or deammoniation, an intermediate species is detected spectroscopically before the fully dehydrated or deammoniated state is obtained. This intermediate has the following spectroscopic characteristics: (1) an EPR spectrum with 'reversed' g-values ($g_\perp > g_\parallel$) [9,19]; (2) the maximum absorption in the DRS spectrum is in the range 10 500–12 500 cm^{-1}, to be compared with the absorption range 10 500–15 000 cm^{-1} for the dehydrated counterparts [7]. There is no agreement on the structure of this intermediate species. It is thought to be a pseudo-tetrahedral complex of the type $(O_l)_3—Cu^{2+}—L$ (where O_l = lattice oxygen and L = NH_3, H_2O). The site proposed for such complexes is the oxygen six-ring [7,9]. It was also proposed that the intermediate is a trigonal bipyramidal complex with Cu^{2+} coordinating to three oxygens of the six-ring, and to one H_2O or NH_3 in the supercage and one H_2O or NH_3 in the sodalite cage [19].

To study the interaction of Cu(II)Y with H_2O and NH_3, the ligand field spectra of Cu(II)Y, obtained after saturation with H_2O and NH_3 and during gradual desorption, were measured by DRS. To interpret these electronic spectra, DFT and CASPT2 calculations were performed. The structure of several $[Cu(NH_3)_y(H_2O)_x]^{2+}$ complexes, representing possible adsorption complexes of Cu^{2+} in the fully and partially hydrated and ammoniated zeolites, was optimized using DFT. CASPT2 spectra of these models were calculated. Calculations were also performed on large cluster compounds, representing complexes of H_2O or

NH_3 with Cu^{2+} in the six-ring site, in order to study the effect of an adsorbing ligand on the deformations induced in the six-ring by the presence of the transition metal ion. The results of the CASPT2 calculations will be compared with the experimental DRS spectra, in order to identify the possible adsorption complexes of H_2O and NH_3 on Cu^{2+} in zeolite Y.

2. Experimental methods

NaY of Ventron with a Si/Al ratio of 2.51 and a cation exchange capacity (CEC) of 4.30 meq g^{-1} was used for ion exchange with Cu^{2+}. The procedure was as follows: 2.5 g zeolite material was used for 1 l of exchange solution, containing the appropriate amount of $CuCl_2.2H_2O$ (UCB) for obtaining a 0.5 Cu^{2+} uc^{-1} (unit cell) loading. At small exchange levels ($Cu/Na < 0.01$), the ion exchange reaction can be considered as complete [40]. The exchange reaction was carried out at room temperature for 24 h, and afterwards, the solid material was separated from the liquid by centrifugation. The material was washed chloride-free and dried at 60°C.

The freshly prepared and dried Cu(II)Y samples were then granulated, and the size fraction 0.25–0.40 mm was loaded in a quartz flow cell with suprasil window for DRS measurements. DRS spectra were taken with a Varian Cary 5 UV-Vis-NIR spectrometer at room temperature. The spectra were recorded against a halon white reflectance standard in the range 200–2500 nm. The computer processing of the spectra consisted of the following steps: (1) subtraction of the baseline; (2) conversion to wavenumber.

The samples were first calcined at 500°C in a flow of oxygen for 6 h and then flushed with He at room temperature. A DRS spectrum of this dehydrated Cu(II)Y sample was taken. In a second step, either NH_3 or H_2O was adsorbed on dehydrated Cu(II)Y by flowing pure NH_3 or a saturated He stream of H_2O over the sample for 45 min at room temperature, and DRS spectra were measured. Gradual desorption of these hydrated or ammoniated samples was performed by heating the sample in a He stream for 25 min at 25, 50, 100, 150, 200, 250 and 300°C. DRS spectra of all these samples were taken.

3. Theoretical methods

3.1. Models

Calculations were performed on $[Cu(NH_3)_y(H_2O)_x]^{2+}$ complexes, and on two cluster models representing the six-ring site: $CuO_6Si_{6-x}Al_x(OH)_{12}(L)^{(2-x)+}$ and $CuO_6Si_{6-x}Al_xH_{12}(L)^{(2-x)+}$, where $L = H_2O$ or NH_3 and $x = 1, 2$. The models of the six-ring site are shown in Fig. 1. Fig. 1(A) shows a model in which the dangling bonds of the silicon or aluminum atoms are terminated by OH groups, while in the model shown in Fig. 1(B), hydrogen atoms are used instead. The Si/Al ratio for zeolite Y is about 2.5, so models were studied with one and two aluminum atoms in the six-ring. According to the Loewenstein rule [20], Al—O—Al linkages are forbidden, and in the case of two aluminum atoms in the six-ring, the aluminums were placed such that they were intervened by either one or two silicon atoms. Four types of oxygens may be distinguished: O_A and O_B are oxygens in the six-ring surrounding copper, O_C denotes the oxygens belonging to the dangling OH groups in the large models, and O_D corresponds to an oxygen atom in an adsorbing water molecule.

3.2. Geometry optimizations

Geometry optimizations were performed with density functional theory, using the Turbomole code [21]. It was shown in our previous study that the B3LYP functional gives better structures than BP86 for Cu^{2+}-clusters [6], so B3LYP was used in all calculations. The basis sets from Schäfer et al. [22] were employed: for copper, the double-ζ basis set was chosen and enhanced with diffuse p, d, and f functions (with exponents 0.174, 0.132 and 0.390, respectively). For O_A, O_B, O_D, and N, and the hydrogens of the adsorbing molecules, the triple-ζ basis sets with one polarization function (exponent 1.20 for oxygen, 1.00 for nitrogen and

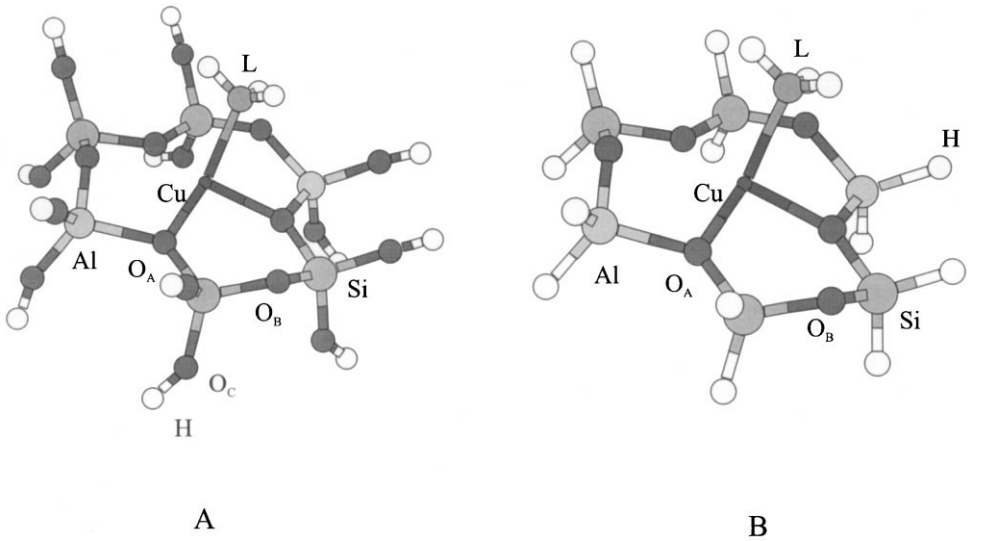

Fig. 1. Models for Cu^{2+} on the six-ring site with an adsorbing ligand (L), $CuO_6Si_{6-x}Al_x(OH)_{12}(L)^{(2-x)+}$ models (A) and $CuO_6Si_{6-x}Al_xH_{12}(L)^{(2-x)+}$ models (B).

0.80 for hydrogen) were used, while for all other atoms, a double-ζ basis set was chosen.

The geometry of the $[Cu(H_2O)_6]^{2+}$, $[Cu(NH_3)_4]^{2+}$, $[Cu(NH_3)_4(H_2O)_x]^{2+}$ complexes (with $x=1$, 2) was fully optimized within the symmetry restrictions of their point group (C_i, D_{2d} and C_{2v} respectively). The $CuO_6Si_{6-x}Al_x(OH)_{12}(L)^{(2-x)+}$ clusters [Fig. 1(A)] used to model adsorption complexes on the Cu^{2+} six-ring sites were optimized without any symmetry restrictions. However, the following restrictions were imposed to mimic the rigidity of the surrounding zeolite framework: the O_C atoms were kept fixed at their positions from XRD [23], and the orientation of the O_C—H bonds was kept fixed towards the next layer of Si, Al in the crystal. The O_C—H bond distances were optimized, and the entire $CuO_6Si_{6-x}Al_x(L)$ cluster was allowed to relax. This optimization procedure is similar to what was called optimization step 4 in our previous studies [4–6], the only difference in this study being the presence of the adsorbing ligand.

For the calculation of the electronic spectra, the smaller models, shown in Fig. 1(B), were used. As was shown in a previous study [4], the presence of either H or OH as terminating groups does not affect the calculated exitation energies of the metal-centered ligand field states to any significant extent, and the use of the smaller models considerably reduces the necessary computational effort. Apart from the different terminating groups, the structures of the smaller models are the same as the corresponding large models. They are obtained by substituting the OH by H groups and reoptimizing only the Si,Al—H bond lengths.

3.3. Calculation of CASPT2 spectra

The spectra of all considered models were calculated using multiconfigurational perturbation theory based on a CASSCF wavefunction, i.e. the CASPT2 method [24]. The MOLCAS-4 software [25] was used, and the basis sets employed are of the generally contracted ANO (atomic natural orbital) type [26] (labeled as ANO-s in the MOLCAS basis set library). The following contractions were used: [6s4p3d1f] for Cu, [3s2p1d] for O_A, O_B, O_D, and N, [4s3p] for Si and Al and [2s] for H.

The CASSCF/CASPT2 calculations consist of two steps. First, a CASSCF wavefunction is built by distributing a limited number of valence electrons over the orbital active space. In all calculations, we include the five metal 3*d* orbitals in the

active space, but also a second, virtual d-shell was added, to account for the 3d 'double-shell' effect, due to the large number of 3d electrons. Non-dynamical correlation effects are also connected to the strong σ-interaction between the oxygen or nitrogen ligands and the Cu 3d orbital that is singly occupied in the ground state (i.e. the 3d orbital pointing towards these ligands). In order to describe those effects, one molecular orbital, consisting of a combination of the lone-pairs on these ligands, was also included in the active space. As such, the active space includes 11 orbitals, populated with 11 electrons.

Remaining correlation effects are dealt with in the second, CASPT2 step, where the CASSCF wave function is the reference function. In the CASPT2 step, all electrons originating from the Cu 3*p*, 3*d*, Si, Al 3*s*, 3*p*, O, N 2*s*, 2*p* and H 1*s* orbitals are correlated. In order to deal with intruder states, a level-shift of 0.3 Hartree, together with a back correction [27,28] was employed.

The CASSCF/CASPT2 calculations were performed in C_i symmetry for $[Cu(H_2O)_6]^{2+}$, and in C_{2v} symmetry for the $[Cu(NH_3)_4(H_2O)_x]^{2+}$ complexes (with $x=1,2$). In the case of $[Cu(NH_3)_4]^{2+}$, the full point group symmetry of the complex is D_{2d}, but since only Abelian point groups are accepted by the MOLCAS code, calculations were performed using D_2 symmetry. Additional symmetry restrictions were imposed to prevent mixing between orbitals belonging to different representations in the parent symmetry groups. In Cu^{2+} complexes, five doublet states arise from the distribution of the nine d-electrons over the 3*d* orbitals. State-average CASSCF calculations were performed, including these five doublet states, followed by a CASPT2 calculation on each state. An exception was made for the $[Cu(NH_3)_4(H_2O)_x]^{2+}$ complexes (with $x=0$, 1, 2), where, for each state, a CASSCF wavefunction was optimized.

Oscillator strengths were obtained by calculating the transition dipole moments, using the CAS state-interaction method [29] and combining them with CASPT2 excitation energies. The calculated oscillator strengths have been included in the tables where appropriate. It should be noted, however, that these results should not be considered an absolute measure of the intensity to be expected for the corresponding excitation. Indeed, most of the intensity of d–d transitions in transition metal systems stems from vibronic coupling, which is not included in our calculations. We will see that the calculated oscillator strengths are indeed small (in the order of 10^{-5}) in all cases [or even become zero in the case of the centrosymmetric $Cu(H_2O)_6^{2+}$ complex]. This also means that the errors on the calculated results may be rather large. As such, the reported values should be taken as qualitative rather than quantitative.

When considering d–d transitions in transition metal systems, scalar relativistic effects may be considered negligible (they only become important when the number of 3d electrons is altered in the transition). Spin–orbit coupling may, however, have some importance, and was therefore included in our calculations. The calculation of the spin–orbit couplings was performed by means of an effective one-electron operator

$$\hat{H}_{so} = Z_{eff}\frac{\alpha^2}{2}\sum_i \frac{1}{r^3}\hat{l}_i \cdot \hat{s}_i,$$

where Z_{eff} is an effective charge and α the fine structure constant [30]. A value of $Z_{eff}=17.1$ (in atomic units of charge) was obtained from a set of test calculations on the free Cu^{2+} ion, where the effective charge was scaled until optimum accordance with the experimental spectrum was obtained. In the present procedure to calculate the spin-orbit couplings, one set of orbitals describing all states is required. For model clusters without symmetry, the average CASSCF orbitals were used. For models with symmetry, the orbital set was constructed from a weighted average of the density matrices resulting from the CASSCF calculations. The different states, between which the spin–orbit coupling was calculated, were then constructed from a full CI expansion in this orbital set, using the active space (11 electrons in 11 orbitals) described above. The corresponding wavefunctions were used to construct the off diagonal elements of the spin–orbit matrix. For the diagonal elements, CASPT2 energies were used, obtained from CASPT2 calculations where the same wavefunctions constituted the reference.

Table 1
Survey of the electronic transitions of dehydrated, (partially) ammoniated and (partially) hydrated 0.5 Cu^{2+} uc^{-1} Cu(II)Y

Sample treatment	Absorption bands (cm^{-1})
After heating at 500°C for 6 h in O_2	9500 (sh); 10 800; 12 300 (sh); 14 900 (sh)
Calcined sample after adsorption of NH_3 at room temperature	9500 (sh); 10 800 (sh); 15 800
After heating the ammoniated sample in He at 200°C	10 500; 12 500 (sh); 15 800 (sh)
After heating the ammoniated sample in He at 250°C	10 500; 12 500 (sh)
Calcined sample after adsorption of H_2O at room temperature	10 400 (sh); 11 400 (sh); 12 500
After heating the hydrated sample in He at 150°C	10 700 (sh); 11 100; 12 500 (sh)

4. Results and discussion

4.1. Diffuse reflectance spectroscopy

The electronic transitions of dehydrated, (partially) ammoniated and (partially) hydrated 0.5 Cu^{2+} uc^{-1} Cu(II)Y are summarized in Table 1. The spectra are similar to those published previously [7]. Fig. 2(A) shows the DRS spectrum of a dehydrated Cu(II)Y sample. The spectrum is characterized by a broad band with a maximum at about 10 800 cm^{-1} and shoulders at about 9500, 12 300 and 14 900 cm^{-1}. The sharp band located at 7300 cm^{-1} corresponds to the first overtone vibration of the terminal silanol groups of the zeolite.

After saturation of the dehydrated Cu(II)Y sample with NH_3 at room temperature, the d–d transitions are shifted to a higher energy, and a broad band with a maximum at 15 800 cm^{-1} is observed [Fig. 2(B)]. In the NIR region, the sharp bands up to 8000 cm^{-1} are assigned to the overtone and combination bands of adsorbed NH_3. Upon heating the ammoniated sample in He, the band centered at 15 800 cm^{-1} gradually disappears [Fig. 2(C)], and at 250°C, the spectrum is characterized by a band at about 10 500 cm^{-1} and a shoulder at 12 500 cm^{-1} [Fig. 2(D)]. Further heating at higher temperatures results in a DRS spectrum typical for a dehydrated Cu(II)Y sample.

Similar observations are made for a dehydrated Cu(II)Y sample treated with a H_2O saturated He stream at room temperature (Fig. 3). The fully hydrated Cu(II)Y sample exhibits the typical absorption band centered at 12 500 cm^{-1} and with shoulders at about 10 400 and 11 400 cm^{-1}

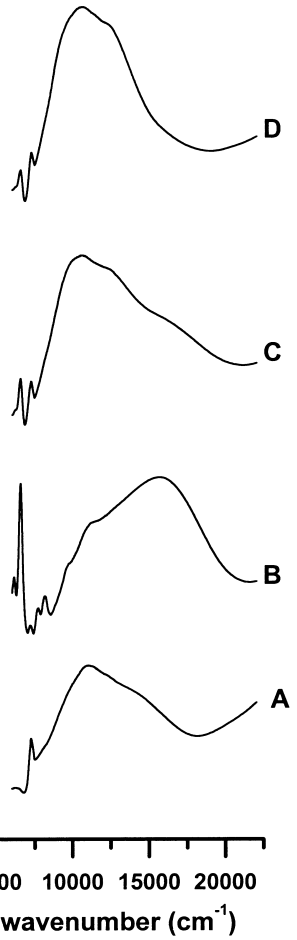

Fig. 2. DRS spectra of 0.5 Cu^{2+} uc^{-1} Cu(II)Y: (A) after heating at 500°C for 6 h in O_2; (B) calcined sample after adsorption of NH_3 at room temperature; (C) after heating the ammoniated sample in He at 200°C and (D) after heating the ammoniated sample in He at 250°C.

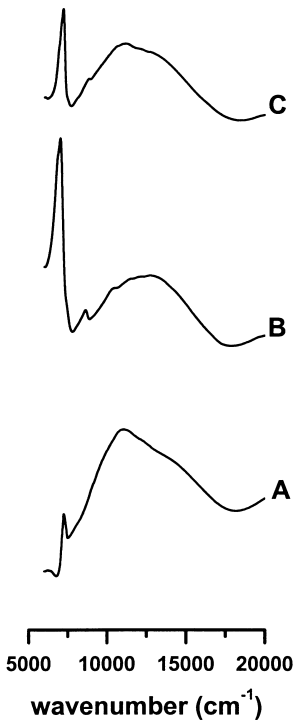

Fig. 3. DRS spectra of 0.5 Cu^{2+} uc^{-1} Cu(II)Y: (A) after heating at 500°C for 6 h in O_2; (B) calcined sample after adsorption of H_2O at room temperature and (C) after heating the hydrated sample in He at 150°C.

[Fig. 3(B)]. The sharp and relatively intense bands located at 6800 and 8600 cm^{-1} correspond to the overtone and combination vibrations of the adsorbed H_2O. Upon heating, the d–d band centered at 12 500 cm^{-1} shifts towards a lower energy with the new maximum at about 11 100 cm^{-1} [Fig. 3(C)]. The original DRS spectrum is restored after heating at 300°C in He.

4.2. Theoretical calculations

4.2.1. Fully hydrated Cu(II) Y

The first cluster studied is the $[Cu(H_2O)_6]^{2+}$ complex, which can be present in the fully hydrated Cu(II)Y zeolite. The optimized geometry of this complex is shown in Fig. 4(A). The structure can be described as an axially distorted octahedron, with four Cu—O bonds of 2.02 Å and two longer Cu—O bonds of 2.29 Å. These bond lengths can be compared with results obtained by XRD of a $CuSO_4.6H_2O$ sample, where the copper ion is surrounded by six water molecules in a distorted octahedral symmetry with Cu—O distances of 1.96, 2.07 and 2.29 Å [17]. The structure of $[Cu(H_2O)_6]^{2+}$ in Cu—ZSM-5 has been studied with ENDOR at 4 K, and Cu—O distances of 2.04 Å for the four equatorial, and 2.19 Å for the two axial oxygens were estimated [17]. These Cu—O distances correspond very well with our DFT results. It should be noted that the distorted octahedron corresponds with one of three (equivalent) minima on the potential energy surface. Elongation along any of the three cartesian coordinates is possible, and at room temperature, the $[Cu(H_2O)_6]^{2+}$ complex is believed to undergo a dynamic Jahn–Teller distortion [31].

The electronic spectrum of the $[Cu(H_2O)_6]^{2+}$ complex, calculated with CASPT2, is presented in Table 2. The symmetry of this complex is C_i, i.e. centrosymmetric with only an inversion center. Since all ligand field states are *gerade* (i.e. of A_g symmetry), electronic transitions between them are dipole-forbidden, and their intensity only arises from vibronic coupling. Without spin–orbit cou-

Table 2
CASPT2 spectrum (in cm^{-1}) of the $[Cu(H_2O)_6]^{2+}$ and $[Cu(NH_3)_4]^{2+}$ complexes, with and without inclusion of spin orbit coupling (s.o.c.), and oscillator strengths (o.s.) of the transitions

$[Cu(H_2O)_6]^{2+}$			$[Cu(NH_3)_4]^{2+}$			
Term	No s.o.c.	With s.o.c.	Term	No s.o.c.	o.s.	With s.o.c.
X^2A_g	0	0	X^2B_2	0		0
b^2A_g	7388	7153	a^2B_1	14 598	0	14 413
c^2A_g	8840	8548	a^2E	16 006	2.5×10^{-6}	15 972
d^2A_g	9300	9769				16 117
e^2A_g	10 118	10 707	a^2A_1	19 414	3.2×10^{-4}	19 776

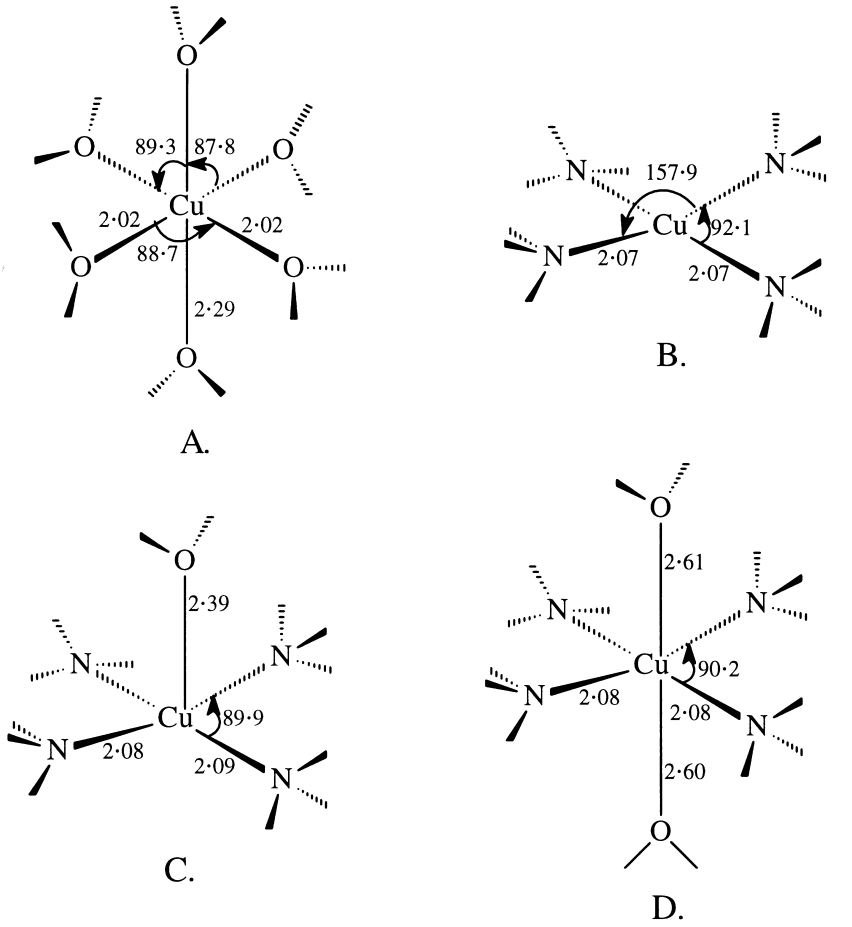

Fig. 4. Optimized geometries for $[Cu(H_2O)_6]^{2+}$ (A), $[Cu(NH_3)_4]^{2+}$ (B), $[Cu(NH_3)_4(H_2O)]^{2+}$ (C) and $[Cu(NH_3)_4(H_2O)_2]^{2+}$ (D); distances in angstroms, angles in degrees.

pling, the highest transition is calculated at 10 000 cm^{-1}. The effect of spin–orbit coupling on the CASPT2 spectrum is relatively small. The difference between the d–d transitions is increased such that the highest transition is now calculated at 10 700 cm^{-1}, in fairly good agreement with the experimentally observed bands at 10 400 cm^{-1}, 11 400 cm^{-1} and 12 500 cm^{-1} in fully hydrated Cu(II)Y. The difference with the experimental spectrum must probably be attributed to deficiencies of the CASPT2 method, since also in a $(NH_4)_2Cu(H_2O)_6(SO_4)_2$ solution, the highest d–d transitions of the $[Cu(H_2O)_6]^{2+}$ complex are observed at 12 350 cm^{-1} [31].

4.2.2. Cu(II) Y, saturated with NH_3

The second complex studied is the $[Cu(NH_3)_4]^{2+}$ complex. The structure of this complex is shown in Fig. 4(B), together with the most important geometrical parameters. The geometry of the complex is not exactly square planar, as described in several articles on the adsorption of NH_3 in Cu^{2+} loaded zeolites [8–10], but is instead found to have D_{2d} symmetry, and an almost planar structure. The N—Cu—N angle between two neighboring nitrogens is 92.1, while the angle between two opposite nitrogens is 157.9. The Cu—N bond lengths are 2.07 Å. This bond distance is in line with the Cu—N distance, determined by XRD in

various $Cu(NH_3)_4X_2$ complexes, ranging between 1.99 and 2.16 Å [32]. The CASPT2 spectrum of the $[Cu(NH_3)_4]^{2+}$ complex is shown in Table 2. Transitions are calculated at 14 400, 16 000 and 19 800 cm^{-1}. Within D_{2d} symmetry, the transitions to ^2E and $^2A_1$ are symmetry-allowed, and the highest oscillator strength is found for the transition to $^2A_1$ at 19 800 cm^{-1}. No transitions as high as 19 800 cm^{-1} are observed in the experimental spectrum of Cu^{2+} in zeolite Y after saturation with NH_3. Instead, a band centered at 15 800 cm^{-1} is found. The difference between these two results, 4000 cm^{-1}, is too large to be caused by limitations of the CASPT2 method. The CASPT2 method is known to be able to predict relative energies of different ligand field states in transition metal systems with an accuracy better than 2500 cm^{-1} [33]. Furthermore, transitions in the region of 19 000 cm^{-1} are often observed in experimental ligand field spectra of Cu^{2+} complexes with four nitrogen-containing ligands in a square planar environment. For example, square planar CuN_4 chromophores have absorption spectra between 18 000 and 21 000 cm^{-1} [31], and the diffuse reflectance spectrum of $[Cu(en)_2]^{2+}$ loaded zeolite X and Y (en = ethylenediamine) shows a band at 18 300 cm^{-1} [34].

We therefore conclude then that the $[Cu(NH_3)_4]^{2+}$ complex, as described above, is unlikely to be present in Cu(II)Y, saturated with NH_3. Instead, the structure of this complex must be influenced by the zeolite environment, most probably by coordination to the lattice oxygens. Indeed, the presence of additional ligands in the coordination sphere of Cu^{2+} in the $[Cu(NH_3)_4]^{2+}$ cation is very likely, and may cause a shift of the ligand field spectrum to lower energies [31]. In aqueous solution, the stepwise formation constant for Cu^{2+} with a fifth ammonia is very small, indicating a negligible tendency to take up more than four NH_3 groups [32]. However, in Cu(II)Y saturated with NH_3, coordination to zeolite lattice oxygens may still occur.

In order to examine this possibility, the geometry of two $[Cu(NH_3)_4(H_2O)_x]^{2+}$ complexes was optimized (with $x = 1, 2$). In these complexes, the water ligands are now used as a model for the zeolite lattice oxygens. In the $[Cu(NH_3)_4(H_2O)]^{2+}$ model, one water ligand represents the presence of one lattice oxygen. A possible coordination to a second oxygen donor was also considered by using a $[Cu(NH_3)_4(H_2O)_2]^{2+}$ complex. In several DFT studies concerning Cu—ZSM-5, water ligands have already been used to model lattice oxygens in zeolites [35–37]. The results have indicated that, in most cases, the water ligand models capture the essential features of the interaction between the zeolite oxygens and the copper ion.

The $[Cu(NH_3)_4(H_2O)_x]^{2+}$ complexes have C_{2v} symmetry and are shown in Fig. 4(C) and (D). In both models, the coordination of the H_2O ligands leaves the Cu—N distances unaffected. The N—Cu—N angles are close to 90°, so the geometry of the $[Cu(NH_3)_4]^{2+}$ complex becomes square planar when one or two H_2O ligands are added. For the $[Cu(NH_3)_4(H_2O)]^{2+}$ cluster, a Cu—O distance of 2.39 Å is calculated. In the model with two H_2O ligands, the Cu—O distances are significantly longer (2.60 and 2.61 Å). The geometry of the $[Cu(NH_3)_4(H_2O)_2]^{2+}$ complex can be described as a tetragonally distorted octahedron.

Table 3
CASPT2 spectrum (in cm^{-1}) after inclusion of spin orbit coupling, oscillator strengths (o.s.) of the transitions

$[Cu(NH_3)_4(H_2O)]^{2+}$			$[Cu(NH_3)_4(H_2O)_2]^{2+}$		
Term	Energies	o.s.	Term	Energies	o.s.
X^2A_1	0		X^2A_1	0	
a^2A_2	14 432	0	a^2A_2	14 372	0
a^2B_1	15 714	1.91×10^{-5}	a^2B_1	15 443	2.80×10^{-7}
a^2B_2	16 177	4.04×10^{-5}	a^2B_2	15 984	6.43×10^{-8}
b^2A_1	17 836	2.50×10^{-5}	b^2A_1	17 454	2.15×10^{-5}

The CASPT2 spectrum of the $[Cu(NH_3)_4(H_2O)]^{2+}$ complex is presented in Table 3. The d–d transitions are found at energies ranging from 14 400 to 17 800 cm^{-1}. The lowest transition to $^2A_2$ is symmetry-forbidden. The most intense transition is observed at 16 200 cm^{-1}, in very good agreement with the diffuse reflectance spectrum of Cu(II)Y, saturated with NH_3. For the $[Cu(NH_3)_4(H_2O)_2]^{2+}$ complex, d–d transitions at 17 400 cm^{-1} are calculated. This is also in agreement with the experimental electronic spectrum of $[Cu(NH_3)_4(H_2O)_2]^{2+}$ cations in aqueous solution, where a band at 16 000–17 000 cm^{-1} is observed [32]. From the calculations, it thus appears that if Cu(II) zeolite Y is saturated with NH_3, the Cu^{2+} ions coordinate with four NH_3 ligands, but a coordination with one or two lattice oxygens is still present. Obviously, from the present study, we are not able to predict which lattice oxygens in zeolite Y are involved.

4.2.3. Partially dehydrated and deammoniated Cu(II) Y

The structures obtained with B3LYP-DFT for the different $CuO_6Si_{6-x}Al_x(OH)_{12}(L)^{(2-x)+}$ clusters (L = H_2O, NH_3 and $x = 1$ or 2) and for the corresponding clusters without adsorbant are shown in Table 4. The labeling of the six O_A,O_B oxygens is indicated in Fig. 5, showing the structure of the central $CuO_6Si_{6-x}Al_x$ ring in the absence of L. Table 4 also includes the binding energy (kJ mol^{-1}) of L to the different rings, defined as:

$$BE = [E(CuO_6Si_{6-x}Al_x(OH)_{12}^{(2-x)+}) + E(L)] - E(CuO_6Si_{6-x}Al_x(OH)_{12}(L)^{(2-x)+}).$$

The local symmetry of the oxygen six-rings obtained from XRD is C_{3v}, with three O_A oxygens found at a distance of 2.14 Å and three O_B oxygens at a longer distance, 2.85 Å [23]. However, the

Table 4
Structure and binding energy (BE) of the $CuO_6Si_{6-x}Al_x(OH)_{12}L^{(2-x)+}$ clusters, optimized using (B3LYP) DFT

	A ($x=1$)[a]				B ($x=2$)[a]				C ($x=2$)[a]			
	No L	L = H_2O	L = NH_3	No Cu no L	No L	L = H_2O	L = NH_3	No Cu no L	No L	L = H_2O	L = NH_3	No Cu no L
BE (kJ mol^{-1})[b]		71.0	112.8			80.3	109.6			64.8	96.2	
R(Cu−O_{A1}) (Å)	1.97	1.98	2.00		1.86	132.0	139.1		2.03	2.20	2.29	
R(Cu−O_{A2}) (Å)	2.37	2.52	2.68		2.47	2.80	2.78		2.08	2.05	2.01	
R(Cu−O_{A3}) (Å)	1.88	1.89	1.90		1.89	1.92	1.93		1.90	1.91	1.94	
R(Cu−O_{B1}) (Å)	3.34	3.33	3.34		3.43	3.49	3.46		3.39	3.28	3.15	
R(Cu−O_{B2}) (Å)	2.07	2.07	2.08		2.10	2.07	2.14		2.21	2.37	2.67	
R(Cu−O_{B3}) (Å)	3.22	3.23	3.26		3.21	3.20	3.23		3.13	3.02	3.02	
R(Cu−L) (Å)		2.14	2.05			2.06	2.04			2.13	2.01	
O_{A1}−Cu−O_{A2} (°)	106.9	104.0	100.0		107.7	100.3	100.4		114.2	112.3	111.3	
O_{A1}−Cu−O_{A3} (°)	148.9	144.9	140.3		150.8	141.3	139.3		142.2	129.1	118.5	
O_{A2}−Cu−O_{A3} (°)	102.8	100.3	96.9		99.3	92.8	93.6		102.3	104.1	106.8	
O_{A1}−Cu−L (°)		103.5	113.0			1.89	1.89			85.1	86.6	
O_{A2}−Cu−L (°)		78.0	74.4			97.3	72.3			89.8	94.4	
O_{A3}−Cu−L (°)		106.0	106.0			70.3	101.8			130.1	136.1	
O_{B2}−Cu−L (°)		108.8	122.1			121.4	118.9			99.6	100.2	
T−O_{A1}−T ()	133.7	134.2	134.0	140.7	131.9	125.3	124.4	127.3	135.0	137.1	135.6	132.0
T−O_{B3}−T (°)	147.3	147.9	147.1	145.4	140.9	138.5	131.8	148.3	140.3	138.6	139.5	146.1
T−O_{A2}−T (°)	127.0	130.5	133.2	141.1	129.3	135.3	135.3	134.6	119.7	121.4	124.0	126.0
T−O_{B1}−T (°)	144.2	144.2	144.0	140.3	141.9	142.6	142.7	141.1	137.8	138.1	138.9	139.5
T−O_{A3}−T (°)	126.6	127.5	127.6	130.5	128.1	128.1	128.5	119.4	127.3	127.4	126.7	124.5
T−O_{B2}−T (°)	147.6	146.6	146.9	138.6	148.5	146.4	145.8	136.1	148.2	144.2	142.9	143.7

[a] For the labeling of the oxygens and the position of the aluminums in structures B and C, see Fig. 5(b).
[b] For the definition of the binding energy, see text.

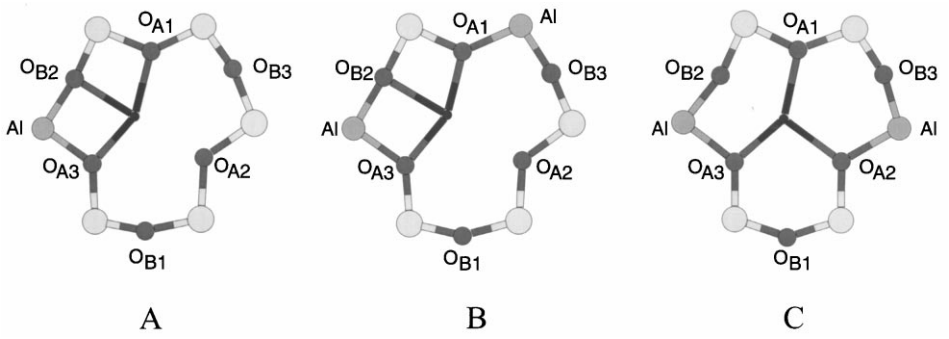

Fig. 5. Labeling of the oxygens in the six-ring models containing one (A) and two (B, C) aluminums.

calculated structures reveal strong local deformations of the six-rings. From the calculated structural data for the different cluster models, it is clear that these deformations serve two purposes, viz. (1) to provide an additional short Cu—O bond, thus giving Cu^{2+} a coordination number of four instead of three, and (2) to provide as many Cu—O bonds as possible, containing oxygens bound to one of the available aluminums. This is illustrated by Table 4 and Fig. 5. In all three cases, the bond distance between copper and O_{B2}, bound to one of the aluminums, is strongly reduced as compared to the crystal value, to 2.07–2.21 Å. In the ring with only one aluminum (cluster A in Fig. 5 and Table 4), the central copper is pulled so strongly towards O_{B2} that the Cu—O_{B2} bond becomes shorter than the opposite Cu—O_{A2} bond, 2.07 Å versus 2.37 Å. This preference of Cu^{2+} for O_{B2} over O_{A2} is obviously related to the fact that O_{B2} is bound to aluminum, whereas O_{A2} is bound between two silicons. The fact that Cu^{2+} causes a distortion in the six-ring can clearly be observed when the values of T—O—T angles in clusters containing Cu^{2+} are compared with rings, optimized without Cu^{2+} (Table 4). For structure A, the T—O_A—T angles are reduced due to the presence of the metal ion, while T—O_B—T angles systematically become larger.

When a second silicon is replaced by an aluminum, two different situations can occur. In the model shown in Fig. 5(B), the presence of the second aluminum does not lead to any strong alterations of the structure as compared to cluster A, except for a shortening by 0.11 Å of the Cu—O_{A1} bond (O_{A1} being bound to the second aluminum) at the expense of Cu—O_{A2} and Cu—O_{B1}. However, in the cluster shown in Fig. 5(C), the second aluminum is bound to O_{A2} and prevents the weakening of the Cu—O_{A2} bond in favor of Cu—O_{B2}. As such, we find a considerably shorter Cu—O_{A2} and a considerably longer Cu—O_{B2} bond in the cluster shown in Fig. 5(C) than in the other two structures. This third structure is on the whole considerably less distorted from the average trigonal structure obtained from XRD. This can also be seen from the changes in the T—O—T angles between the clusters with and without Cu^{2+}, which are smaller than in the case of structures A and B.

When adsorbing an external ligand, the Cu^{2+} ion at least partly gives up one of its bonds to the six-ring oxygens. From Table 4, one can see that indeed only three short Cu—O bonds are found in the structures with L = H_2O, NH_3. A fourth bond is now instead formed with the extra-lattice ligand. Which of the bonds is given up depends on the original structure: in clusters A and B, the Cu—O_{A2} is further released as compared to the naked cluster, while after adsorption of H_2O or NH_3 to cluster C, the Cu—O_{B2} bond is released, such that the original deformation of the six-ring is relaxed. From the binding energies in Table 4, we also notice that in the case of two aluminums, the distribution found in structure B gives rise to a considerably stronger Cu—L bond than the alternative distribution of structure C. The strongest Cu—NH_3 bond is calculated for the ring with only one aluminum, while H_2O binds strongest to

copper in a six-ring with two aluminums, distributed as in structure B. It is also clear that NH_3 systematically gives a stronger bond to Cu^{2+} than H_2O in the considered oxygen six-rings, in agreement with the observations from Naccache and Ben Taarit [13].

The calculated spectra of the three considered six-rings, with and without an external ligand, are presented in Table 5. Again, a distinction can be made between clusters A, B, containing a short $Cu-O_{B2}$ bond, and cluster C, with a strong $Cu-O_{A2}$ but much weaker $Cu-O_{B2}$ bond. As one can see, the latter structure gives rise to a slightly weaker ligand field than the other two structures, both with and without L. The calculated spectra of structures A, B are in excellent agreement with the experimental band positions in the DRS spectra (Table 1). Without H_2O or NH_3, all fair bands are well reproduced. For structure C, the calculations do not show a transition at 12 500 cm^{-1}, but instead, two excitations are calculated around 10 500 cm^{-1}. The calculations also nicely reproduce the observed red shift in the spectra of partially dehydrated or deammoniated Cu(II)Y. The highest and strongest transition is now calculated at around 12 500 cm^{-1} in structure B, for both NH_3 and H_2O, in agreement with experiment. Slightly lower excitation energies are found for the clusters with only one aluminum. All calculated excitation energies of cluster C are even lower, the highest transition being calculated at 10 400 cm^{-1}. However, considering that the binding energy of both NH_3 and H_2O is considerably lower for this than for the other two clusters, zeolite–adsorbant complexes with an aluminum distribution as in cluster C may be expected to be less abundantly present, and provide only a weak contribution to the observed electronic spectrum. Finally, it should be noted that, even if the results of our calculations on clusters with only one NH_3 or H_2O conform with the experimental observations, we cannot exclude the possibility that a contribution to the latter may also be provided by adsorption complexes containing more than one external ligand. This possibility is currently being investigated.

Table 5
CASPT2 spectra (in cm^{-1}), including the effect of spin–orbit coupling, of the different $CuO_6Si_{6-x}Al_x(OH)_{12}L^{(2-x)+}$ clusters (calculated oscillator strengths ($\times 10^{-5}$) of the different excitations are given within parentheses)

State	Structure A $x=1$	Structure B[a] $x=2$	Structure C[a] $x=2$
No L			
b^2A	9476 (3.96)	9334 (1.73)	7828 (0.92)
c^2A	10 779 (0.28)	10 342 (0.65)	10 141 (0.21)
d^2A	12 348 (0.78)	12 775 (1.39)	10 827 (0.85)
e^2A	15 353 (0.50)	15 346 (0.28)	14 575 (0.83)
$L=H_2O$			
b^2A	7168 (0.66)	7424 (0.19)	5325 (2.22)
c^2A	8511 (0.77)	9050 (0.44)	6656 (1.25)
d^2A	9056 (0.78)	10 076 (1.01)	7986 (0.70)
e^2A	11 537 (2.99)	12 654 (7.12)	10 026 (1.14)
$L=NH_3$			
b^2A	6866 (0.93)	7263 (2.29)	5361 (0.52)
c^2A	7720 (0.45)	8764 (1.08)	7384 (1.18)
d^2A	9478 (1.00)	10 054 (0.50)	8478 (2.05)
e^2A	11 936 (7.24)	12 785 (8.08)	10 399 (5.99)

[a] For the position of the aluminums in structures B and C, see Fig. 5.

5. Conclusions

In order to study the interaction of H_2O and NH_3 with Cu^{2+} ions in zeolite Y, the experimental ligand field spectrum of hydrated and ammoniated Cu(II)Y was compared to electronic spectra of model compounds, as calculated by the CASPT2 method. The following conclusions can be drawn from this study:

1. In fully ammoniated Cu(II)Y, an isolated $[Cu(NH_3)_4]^{2+}$ complex is not likely to be present. Such a complex would have its most intense d–d transition at 19 700 cm^{-1}, which is not experimentally observed. Instead, a good agreement between the experimental DRS spectrum and the CASPT2 spectrum of $[Cu(NH_3)_4(H_2O)_x]^{2+}$ complexes (with $x=1, 2$) was obtained. It is concluded that the Cu^{2+} ion in a $[Cu(NH_3)_4]^{2+}$ cation has an additional axial coordination to one or two lattice oxygens of the zeolite. In hydrated Cu(II)Y, distorted $[Cu(H_2O)_6]^{2+}$ complexes are present in the zeolite cages. In these complexes, Cu^{2+} is surrounded by six oxygens in an axially distorted

octahedral symmetry. Since the H_2O ligands can also be used to represent framework oxygens, it may be possible that, also upon complete hydration, the Cu^{2+} ion is not completely detached form the zeolite framework.

2. In the absence of an extra-lattice ligand, the six-ring site of zeolite Y is distorted so that the Cu^{2+} reaches a fourfold coordination with the lattice oxygens. After adsorption of H_2O or NH_3, the weakest Cu—O bond is given up and replaced by a bond with the extra-lattice ligand. The $Cu—NH_3$ bond is found to be considerably stronger than the $Cu—H_2O$ bond.
3. Experimentally, the spectrum of partially dehydrated or deammoniated Cu(II)Y is observed at a lower energy than the spectrum of the completely dehydrated or deammoniated Cu(II)Y. This is confirmed by the CASPT2 results of the six-ring clusters.

Acknowledgements

This investigation has been supported by grants from the Flemish Science Foundation (FWO), the Concerted Research Action of the Flemish Government, and by the European Commission through the TMR program (grant ERBFMRXCT960079). M.G. thanks the Institute for the Promotion of Innovation by Science and Technology in Flanders (IWT) for a research grant.

References

[1] G.M. Rosenblatt, W.L. Worrell (Eds.), Prog. Solid State Chem. Vol. 16, Pergamon Press, Oxford, 1985, p. 1.
[2] W.J. Mortier, Compilation of Extra-framework Sites in Zeolites, Butterworth, London, 1982.
[3] W.M. Meier, D.H. Olson, C. Baerlocher, Atlas of Zeolite Structure Types, fourth ed., Elsevier, Amsterdam, 1996.
[4] K. Pierloot, A. Delabie, C. Ribbing, A.A. Verberckmoes, R.A. Schoonheydt, J. Phys. Chem. B 102 (1998) 10805.
[5] A.A. Verberckmoes, R.A. Schoonheydt, A. Ceulemans, A. Delabie, K. Pierloot, in: 12th Int. Zeolite Conf., Materials Research Proc. (1998) 387.
[6] K. Pierloot, A. Delabie, A.A. Verberckmoes, R.A. Schoonheydt, Proc. DFT Symp., a Bridge Between Chemistry and Physics, Brussels, (1999) in press.
[7] W. De Wilde, R.A. Schoonheydt, J.B. Uytterhoeven, ACS Symp. Ser. 40 (1977) 132.
[8] W.B. Williamson, J.H. Lunsford, J. Phys. Chem. 80 (1976) 2664.
[9] E.F. Vansant, J.H. Lunsford, J. Phys. Chem. 76 (1972) 2860.
[10] D.R. Flentge, J.H. Lunsford, P.A. Jacobs, J.B. Uytterhoeven, J. Phys. Chem. 79 (1975) 354.
[11] P.K. Dutta, R.E. Zaykoski, J. Inorg. Chem. 24 (1985) 3490.
[12] H. Yamashita, M. Matsuoka, K. Tsuji, Y. Shioya, M. Anpo, M. Che, J. Phys. Chem. 100 (1996) 397.
[13] C. Naccache, Y. Ben Taarit, Chem. Phys. Lett. 11 (1971) 11.
[14] J. Turkevich, Y. Ono, J. Soria, J. Catal. 25 (1972) 44.
[15] J. Dědeček, B. Wichterlová, J. Phys. Chem. B 101 (1997) 10233.
[16] Z. Sobalík, J. Dědeček, I. Ikonnikov, B. Wichterlová, Microporous Mesoporous Mater. 21 (1998) 525.
[17] H. Li, D. Biglino, R. Erickson, A. Lund, Chem. Phys. Lett. 266 (1997) 417.
[18] M.P. Attfield, S.J. Weigel, A.K. Cheetham, J. Catal. 170 (1997) 227.
[19] R.G. Herman, Inorg. Chem. 18 (1979) 995.
[20] W. Loewenstein, Am. Miner. 39 (1942) 92.
[21] R. Ahlrichs, M. Bär, M. Häser, H. Horn, C. Kölmel, Chem. Phys. Lett. 162 (1989) 165.
[22] A. Schäfer, H. Horn, R. Aldrichs, J. Chem. Phys. 97 (1992) 2571.
[23] H.S. Lee, K. Seff, J. Chem. Phys. 85 (1992) 397.
[24] K. Andersson, a. Malmqvist, B.O. Roos, J. Chem. Phys. 96 (1992) 1218.
[25] K. Andersson, M.R.A. Blomberg, M.P. Fülscher, G. Karlström, R. Lindh, a. Malmqvist, P. Neogrády, J. Olsen, B.O. Roos, A.J. Sadlej, M. Schütz, L. Seijo, L. Serrano-Andrés, P.E.M. Siegbahn, P.-O. Widmark, MOLCAS Version 4.0, University of Lund, Lund, 1997.
[26] K. Pierloot, B. Dumez, P.-O. Widmark, B.O. Roos, Theor. Chim. Acta 90 (1995) 87.
[27] B.O. Roos, K. Andersson, Chem. Phys. Lett. 245 (1995) 215.
[28] B.O. Roos, K. Andersson, M.P. Fülscher, L. Serrano-Andrés, K. Pierloot, M. Merchán, V. Molina, J. Mol. Struct. (Theochem) 388 (1996) 257.
[29] a. Malmqvist, B.O. Roos, Chem. Phys. Lett. 155 (1989) 189.
[30] C. Ribbing, C. Daniel, J. Chem. Phys. 100 (1994) 6591.
[31] A.B.P. Lever, Inorganic Electronic Spectroscopy, second ed.Elsevier, Amsterdam, 1984.
[32] B.J. Hathaway, A.A.G. Tomlinson, Coord. Chem. Rev. 5 (1970) 1.
[33] B.O. Roos, K. Andersson, M.P. Fülscher, P.Å. Malmqvist, L. Serrano-Andrés, K. Pierloot, M. Merchán, I. Prigogine, S.A. Rice (Eds.), Advances in Chemical Physics: New

Methods in Computational Quantum Mechanics Vol. XCIII, Wiley, New York, 1996, p. 219.
[34] P. Peigneur, J.H. Lunsford, W. De Wilde, R.A. Schoonheydt, J. Phys. Chem. 81 (1977) 1179.
[35] W.F. Schneider, K.C. Hass, R. Ramprasad, J.B. Adams, J. Phys. Chem. 100 (1996) 6032.
[36] R. Ramprasad, K.C. Hass, W.F. Schneider, J.B. Adams, J. Phys. Chem. B 101 (1997) 6903.
[37] H.V. Brand, A. Redondo, P.J. Hay, J. Phys. Chem. B 101 (1997) 7691.
[38] P. Gallezot, Y. Ben Taarit, B. Imelik, J. Catal. 26 (1972) 295.
[39] R.A. Schoonheydt, J. Phys. Chem. Solids 50 (1989) 523.
[40] R.P. Townsend, H. van Bekkum, E.M. Flanigen, J.C. Jansen (Eds.), Studies in Surface Science and Catalysis Vol. 58, Elsevier, Amsterdam, 1991, p. 359.